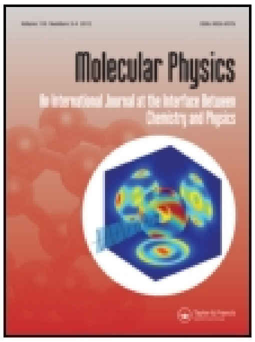

Molecular Physics

An International Journal at the Interface Between Chemistry and Physics

ISSN: 0026-8976 (Print) 1362-3028 (Online) Journal homepage: https://www.tandfonline.com/loi/tmph20

Semi-classical path integral non-adiabatic dynamics: a partial linearized classical mapping Hamiltonian approach

Pengfei Huo & David F. Coker

To cite this article: Pengfei Huo & David F. Coker (2012) Semi-classical path integral non-adiabatic dynamics: a partial linearized classical mapping Hamiltonian approach, Molecular Physics, 110:9-10, 1035-1052, DOI: 10.1080/00268976.2012.684896

To link to this article: https://doi.org/10.1080/00268976.2012.684896

Molecular Physics
Vol. 110, Nos. 9–10, 10–20 May 2012, 1035–1052

Taylor & Francis
Taylor & Francis Group

INVITED ARTICLE

Semi-classical path integral non-adiabatic dynamics: a partial linearized classical mapping Hamiltonian approach

Pengfei Huo[ab] and David F. Coker[ac*]

[a]Department of Chemistry, Boston University, 590 Commonwealth Avenue, Boston, MA 02215, USA; [b]Division of Chemistry and Chemical Engineering, California Institute of Technology, Pasadena, California 91125, USA; [c]School of Physics and Complex Adaptive Systems Laboratory, University College Dublin, Belfield, Dublin 4, Ireland

(*Received 12 February 2012; final version received 5 April 2012*)

A new partially linearized approximate approach to non-adiabatic quantum dynamics is derived based on linearizing the path difference for nuclear degrees of freedom (DOF) in the classical mapping Hamiltonian while keeping quantum interference effects inherent in the forward and backward propagators for the electronic DOF. With this new approach, the non-adiabatic force that acts on the nuclear DOF is a mean force rather than a state dependent force as found in some alternative approaches. Various benchmark examples are explored to test the accuracy of this new approach, and compare its performance with other approaches for a wide range of physical phenomena including: non-adiabatic scattering, excited state conical intersection dynamics, excited state photoisomerization, and excitation energy transfer in realistic condensed phase model systems. Results indicate that, even though the method is based on a ''mean trajectory''-like scheme, it can accurately capture electronic population branching through multiple avoided crossing regions and that the approach offers a robust and reliable way to treat quantum dynamical phenomena in a wide range of condensed phase applications.

Keywords: non-adiabatic dynamics; mapping Hamiltonian; quantum dynamics; linearized semi-classical dynamics

1. Introduction

The mixed quantum-classical strategy for modeling systems in which quantum coherent dynamics and electronically non-adiabatic transitions play important roles describes the nuclear degrees of freedom (DOF) classically or semi-classically, while treating the electronic DOF quantum mechanically with an evolution operator parameterized by trajectories of the nuclear DOF [1]. Though many schemes for implementing this idea have been developed [2,3], fundamental questions arise about the accuracy of dynamics methods that treat the electronic and nuclear DOF on different dynamical footings [4–6]. To overcome this difficulty, the mapping Hamiltonian idea that exactly maps discrete quantum states onto continuous coordinates was proposed by Miller and co-workers [7–9] and enables a consistent treatment for all DOF. This idea replaces the evolution of the electronic subsystem by the dynamics of a system of fictitious mapping harmonic oscillators. With this approach *e.g.*, the quantum amplitude transfer operator transforms as $|\beta\rangle\langle\lambda| \to \hat{a}^{\dagger}_{\beta}\hat{a}_{\lambda}$, where $\hat{a}_{\lambda} = \frac{1}{\sqrt{2\hbar}}(\hat{q}_{\lambda} - i\hat{p}_{\lambda})$, and a general electronic Hamiltonian in the diabatic representation, $\hat{h}_{el} = \sum_{\beta,\lambda} |\beta\rangle\langle\beta|\hat{h}_{el}(\hat{R})|\lambda\rangle\langle\lambda|$, can be rewritten as:

$$\hat{h}_{map}(\hat{R}) = \frac{1}{2\hbar}\sum_{\beta} h_{\beta,\beta}(\hat{R})(\hat{q}^2_{\beta} + \hat{p}^2_{\beta} - \hbar) + \frac{1}{2\hbar}\sum_{\lambda\neq\beta} h_{\beta\lambda}(\hat{R})(\hat{q}_{\beta}\hat{q}_{\lambda} + \hat{p}_{\beta}\hat{p}_{\lambda}) \qquad (1)$$

where $(\hat{P}, \hat{R})$ and $(\hat{p}_{\lambda}, \hat{q}_{\lambda})$ represent the nuclear, and mapping oscillator phase space DOF, respectively. Direct implementation of this mapping Hamiltonian by the stationary phase approximation and classical trajectories encounters a fatal problem when $q^2_{\beta} + p^2_{\beta} < \hbar$, since some of the classical DOF can evolve on an inverted potential surface, proportional to $-h_{\beta,\beta}(R)$ arising from the first term in Equation (1) [10,11]. Moreover, the population, $\rho_{\beta\beta} = \hat{a}^{\dagger}_{\beta}\hat{a}_{\beta} = \frac{1}{2\hbar}(\hat{q}^2_{\beta} + \hat{p}^2_{\beta} - \hbar)$, is not guaranteed to have a positive expected value when the approach is implemented approximately, *e.g.*, with the linearized semi-classical initial value representation (LSC-IVR) applied to multi-state systems [11,12]. This is due to the

---

*Corresponding author. Email: coker@bu.edu

ISSN 0026–8976 print/ISSN 1362–3028 online

http://dx.doi.org/10.1080/00268976.2012.684896
http://www.tandfonline.com

unphysical flow of zero point energy of the mapping harmonic oscillators in the classical limit [13,14]. On the other hand, LSC-IVR linearizes in the difference between forward and backward paths for both the mapping and nuclear DOF. To overcome all these problems, in this paper we outline a method that employs the coherent state representation of the mapping DOF [15,16] and linearize only in the nuclear DOF, allowing different mapping variable paths for the forward and backward propagators, *i.e.*, partial linearization.

The paper is organized as follows: First, in Section 2, the basic theory that underlies the propagation of the density matrix written in terms of discrete quantum states for the electronic subsystem and continuous coordinates for the nuclear DOF is developed in the mapping Hamiltonian formulation giving a path-integral expression that we linearize in the difference between the forward and backward paths of the nuclear DOF to obtain our expressions for the partial linearized density matrix (PLDM) propagation approach. Details of this theoretical development can be found in reference [17]. Next, in Section 3, we explore the accuracy, reliability, and efficiency of the approach by comparing results from different calculations on various model benchmark systems including: multi-state Morse potential models of non-adiabatic molecular photodissociation, various models of excited state conical intersection dynamics applicable to excited state spectroscopy, and a *cis-trans* photoisomerization reaction in solution, as well as multi-state "spin-boson"-like models of electron and excitation energy transfer in condensed phase systems, thus demonstrating the broad applicability of the approach and exploring its limitations for different applications. Finally, our findings are summarized and concluding remarks are presented in Section 4. Appendices are included that offer summaries of various approaches for implementing the mapping Hamiltonian for quantum dynamics enabling theoretical comparison of the present PLDM propagation method to various other techniques.

2. Theory

The quantity of interest is the evolution of the density matrix involving forward and backward propagation:

$$\langle R_t, n_t|\hat{\rho}|R'_t, n'_t\rangle = \sum_{n_0, n'_0} \int \mathrm{d}R_0 \mathrm{d}R'_0 \langle R_t, n_t| e^{-\frac{i}{\hbar}\hat{H}t} |R_0, n_0\rangle \times \langle R_0, n_0|\hat{\rho}(0)|R'_0, n'_0\rangle \langle R'_0, n'_0| e^{\frac{i}{\hbar}\hat{H}t} |R'_t, n'_t\rangle \tag{2}$$

where the total Hamiltonian is $\hat{H} = \hat{P}^2/2M + h_{map}(\hat{R}, \hat{p}, \hat{q})$, and n_t labels the basis states at time t. The propagator matrix elements in discrete path integral form are:

$$\langle R_N, n_t| e^{-\frac{i}{\hbar}\hat{H}t} |R_0, n_0\rangle = \int \prod_{k=1}^{N-1} \mathrm{d}R_k \frac{dP_k}{2\pi\hbar} \frac{dP_N}{2\pi\hbar} e^{\frac{i}{\hbar}S_0} \times \langle n_t| e^{-\frac{i}{\hbar}\epsilon \hat{h}_{map}(R_{N-1})} \ldots e^{-\frac{i}{\hbar}\epsilon \hat{h}_{map}(R_0)} |n_0\rangle \tag{3}$$

where ϵ is a time step, the nuclear kinetic action is

$$S_0 = \epsilon \sum_{k=1}^{N} \left[P_k \frac{(R_k - R_{k-1})}{\epsilon} - \frac{P_k^2}{2M} \right]$$

and $T_{[n_t, n_0]} = \langle n_t| e^{-\frac{i}{\hbar}\epsilon \hat{h}_{map}(R_{N-1})} \ldots e^{-\frac{i}{\hbar}\epsilon \hat{h}_{map}(R_0)} |n_0\rangle$ is the nuclear path dependent quantum transition amplitude.

In the coherent state representation (with coherent state width parameter, $\gamma = 1/2$ and setting units so that $\hbar = 1$), the transition amplitude can be expressed as [15,16]:

$$T_{[n_t, n_0]} = \int \mathrm{d}q_0 \mathrm{d}p_0 \frac{1}{4} (q_{n_t} + ip_{n_t})(q_{n_0} - ip_{n_0}) c_t e^{iS_1(t)} \times e^{-\frac{i}{2}\sum_\beta (q_{\beta t} p_{\beta t} - q_{\beta 0} p_{\beta 0})} e^{-\frac{1}{2}\sum_\beta (q_{\beta 0}^2 + p_{\beta 0}^2)} \tag{4}$$

where $c_t = e^{-\frac{i}{2\hbar}\int_0^t \mathrm{d}\tau \sum_\beta \hat{h}_{\beta\beta}(R)}$, $S_1(t) = \int_0^t L_1(\tau)\mathrm{d}\tau$, with $L_1 = L_1^{cl} + \frac{1}{2}\sum_\beta h_{\beta\beta}(R)$, $L_1^{cl} = \sum_\beta p_\beta \dot{q}_\beta - h_{map}^{cl}(R)$ and

$$h_{map}^{cl}(R, p, q) = \frac{1}{2} \sum_\beta h_{\beta\beta}(R) \left(p_\beta^2 + q_\beta^2 \right) + \frac{1}{2} \sum_{\lambda \neq \beta} h_{\lambda\beta}(R) \left(p_\lambda p_\beta + q_\lambda q_\beta \right). \tag{5}$$

The term $\frac{\hbar}{2}\sum_\beta h_{\beta\beta}(R)$ in the action, S_1, that gives rise to the problem of inverting the potential can be eliminated as this term is canceled exactly by the prefactor, c_t [15,16] leaving $S_1^{cl}(t) = \int_0^t L_1^{cl}(\tau)\mathrm{d}\tau$ in the phase.

An important difference between the approach outlined here and the quasi-classical approximation presented in references [29,30] is that in the quasi-classical method the $-\hbar$ factor in the first term of the full mapping Hamiltonian in Equation (1) is replaced by an *ad hoc* adjustable parameter that attempts to model the zero point energy flow between the quantum and classical subsystems. Subsequently the quasi-classical approach treats all degrees of freedom in the resulting Hamiltonian classically. With the PLDM approach presented here, however, the troublesome $-\hbar$ factor is exactly canceled due to the particular choice of coherent state width parameter and the forward and backward mapping variable paths are treated explicitly. This choice of coherent state width parameter, while providing a numerically stable way of implementing this approach may, however, influence the accuracy due the approximation underlying partial linearization and may lead to an inaccurate description of the zero point energy flow.

The combined forward and backward propagators in Equation (2) can lead to phase cancellation that can cause problems for numerical implementation. Approximate schemes such as Forward Backward (FB) SC-IVR [18] can alleviate these difficulties. Alternatively, here we use the idea of partial linearization [19–21] in the nuclear DOF that involves transforming the forward and backward nuclear path variables, R and R', to mean and difference variables: $\bar{R} = (R + R')/2$ and $Z = (R - R')$ respectively (with similar definitions for the mean and difference nuclear momenta, $\bar{P}$ and Y respectively). The nuclear kinetic action difference becomes: $(S_0 - S'_0) = \bar{P}_N Z_N - \bar{P}_1 Z_0 - \sum_{k=1}^{N-1} (\bar{P}_{k+1} - \bar{P}_k) Z_k - \sum_{k=1}^{N} [\frac{\epsilon}{m} \bar{P}_k - (\bar{R}_k - \bar{R}_{k-1})] Y_k$. The central approximation with this approach involves truncating the phase difference in the combined transition amplitude terms to linear order in Z, based on the assumption that for short times, forward and backward nuclear paths will remain close to each other. This may appear to be a restrictive approximation that will only be valid for very short times for high dimensional problems but such linearization approximations have been shown to be reliable even when forward and backward paths differ significantly in some degrees of freedom [22]. With the linearization approximation, the key term is the classical mapping Hamiltonian difference $\Delta H^{cl}_{map} = [h^{cl}_{map}(R, p, q) - h^{cl}_{map}(R', p', q')]$ which can be written as

$$\Delta H^{cl}_{map} = \Big[h^{cl}_{map}(\bar{R}, p, q) - h^{cl}_{map}(\bar{R}, p', q')] + \frac{1}{2}\Big(\nabla_{\bar{R}} h^{cl}_{map}(\bar{R}, p, q) + \nabla_{\bar{R}} h^{cl}_{map}(\bar{R}, p', q')\Big) Z + \mathcal{O}(Z^2). \tag{6}$$

Using this to expand the action difference in Z, and propagating p and q with $h^{cl}_{map}(\bar{R}, p, q)$ (instead of $h^{cl}_{map}(R, p, q)$ or $h^{cl}_{map}(R', p', q')$), we obtain the following expression: $\sum_\beta p_\beta \dot{q}_\beta - h^{cl}_{map}(\bar{R}, p, q) = \frac{1}{2}\frac{\mathrm{d}}{\mathrm{d}\tau}\big(\sum_\beta p_\beta q_\beta\big)$, and the transition amplitude phase difference, $\Delta S^{cl}_1 = (S^{cl}_1[R(t), q(t), p(t)] - S^{cl}_1[R'(t), q'(t), p'(t)])$ can be expanded as

$$\Delta S^{cl}_1 = \int_0^t \Bigg[\frac{1}{2}\frac{\mathrm{d}}{\mathrm{d}\tau}\sum_\beta (p_{\beta\tau} q_{\beta\tau} - p'_{\beta\tau} q'_{\beta\tau}) + \frac{1}{2}\Big(\nabla_{\bar{R}} h^{cl}_{map}(\bar{R}_\tau, p_\tau, q_\tau) + \nabla_{\bar{R}} h^{cl}_{map}(\bar{R}_\tau, p'_\tau, q'_\tau)\Big) Z_\tau\Bigg] \mathrm{d}\tau + \mathcal{O}(Z^2_\tau). \tag{7}$$

With this result the first term in Equation (7) cancels the boundary terms in $T_{[n_t, n_0]}$ given in Equation (4) and similarly for the backward path transition amplitude, $T'_{[n'_0, n'_t]}$.

Combining the forward and backward phase factors $(e^{i/\hbar(S_0 - S'_0)} T_{[n_t, n_0]} T'_{[n'_0, n'_t]})$ and performing the integrals over $Z_0, \ldots, Z_{N-1}$, gives our approximation for $\rho_{n_t, n'_t}(R, R', t) = \langle \bar{R}_N + \frac{Z_N}{2}, n_t | \hat{\rho}(t) | \bar{R}_N - \frac{Z_N}{2} \rangle$ as

$$\begin{aligned}\rho_{n_t, n'_t}(R, R', t) = \sum_{n_0, n'_0} \int & \mathrm{d}\bar{R}_0 \mathrm{d}q_0 \mathrm{d}p_0 \mathrm{d}q'_0 \mathrm{d}p'_0 G_0 G'_0 \frac{1}{4}(q_{n_0} - ip_{n_0}) \\ & \times (q'_{n'_0} + ip'_{n'_0}) \\ & \times \int \prod_{k=1}^{N-1} \mathrm{d}\bar{R}_k \frac{\mathrm{d}\bar{P}_k}{2\pi\hbar} \frac{\mathrm{d}\bar{P}_N}{2\pi\hbar} (\hat{\rho})^{n_0, n'_0}_W (\bar{R}_0, \bar{P}_1) \frac{1}{4} \\ & \times (q_{n_t} + ip_{n_t})(q'_{n'_t} - ip'_{n'_t}) \\ & \times \prod_{k=1}^{N-1} \delta\left(\frac{\bar{P}_{k+1} - \bar{P}_k}{\epsilon} - F_k\right) \\ & \times \prod_{k=1}^{N} \delta\left(\frac{\bar{P}_k}{M} - \frac{\bar{R}_k - \bar{R}_{k-1}}{\epsilon}\right) e^{\frac{i}{\hbar}\bar{P}_N Z_N}.\end{aligned} \tag{8}$$

Here, $G_0 = e^{-\frac{1}{2}\sum_\beta (q^2_{\beta 0} + p^2_{\beta 0})}$ and $G'_0 = e^{-\frac{1}{2}\sum_{\beta'} (q'^2_{\beta' 0} + p'^2_{\beta' 0})}$ are the initial distributions for the forward and backward mapping variables that satisfy $\dot{q}_{n_t} = \partial h^{cl}_{map}(\bar{R}_t)/\partial p_{n_t}$ and $\dot{p}_{n_t} = -\partial h^{cl}_{map}(\bar{R}_t)/\partial q_{n_t}$, and the nuclear trajectories are determined by a "mean field"-like force resulting from the different forward and backward mapping paths:

$$F_k = -\frac{1}{2}\nabla_{\bar{R}_k}\Big[h^{cl}_{map}(\bar{R}_k, p_k, q_k) + h^{cl}_{map}(\bar{R}_k, p'_k, q'_k)\Big]. \tag{9}$$

The mean nuclear DOF initial distribution is the partial Wigner transform: $(\hat{\rho})^{n_0, n'_0}_W(\bar{R}_0, \bar{P}_1) = \int \mathrm{d}Z_0 \langle \bar{R}_0 + \frac{Z_0}{2}, n_0 | \hat{\rho} | \bar{R}_0 - \frac{Z_0}{2}, n'_0 \rangle e^{-\frac{i}{\hbar}\bar{P}_1 Z_0}$. We use factorized initial conditions, $\rho_0 = \rho^{eq}_{bath}(R)\rho_{sys}$, though the non-separable case can be treated [23,24].

Numerical implementation of Equation (8) involves sampling initial nuclear DOF from $(\hat{\rho})^{n_0, n'_0}_W(\bar{R}_0, \bar{P}_1)$, and mapping variables from the Gaussian functions. However, with the "focused mapping initial condition" [15], the numerical convergence will be improved and typically only requires $\sim 10^4$ trajectories. The accuracy of the focused initial condition sampling will be discussed in detail later in the result section. The product of δ-functions in Equation (8) gives a time-stepping prescription for evolving the mean nuclear DOF with the force in Equation (9). Finally quantum expectation values are computed using Equation (8) and the state projected Wigner distribution:

$$(\hat{\rho})^{n_t, n'_t}_W(\bar{R}_N, \bar{P}_t) = \int \mathrm{d}Z_N e^{-\frac{i}{\hbar}\bar{P}_t Z_N} \left\langle \bar{R}_N + \frac{Z_N}{2}, n_t \middle| \hat{\rho} \middle| \bar{R}_N - \frac{Z_N}{2}, n'_t \right\rangle. \tag{10}$$

We refer to the approach presented above as Partial Linearized Density Matrix (PLDM) propagation [17].

The PLDM propagation scheme is a "mean trajectory" approach, but according to Equation (9) it is different from "Ehrenfest" or LSC-IVR dynamics where the force on the nuclear DOF depends only on one set of mapping variables as $F^{Eh} = -\sum_{\beta} \frac{1}{2\hbar}[(q_{\beta}^{2}+p_{\beta}^{2}-1)\nabla_{R}h_{\beta,\beta}+\sum_{\lambda\neq\beta}(q_{\beta}q_{\lambda}+p_{\beta}p_{\lambda})\nabla_{R}h_{\beta,\lambda}]$ [18,25]. The PLDM force in Equation (9) is governed by both forward and backward mapping DOF, however, the scaling of the computational cost of the PLDM approach with increasing number of classical degrees of freedom is linear, similar to the LSC-IVR approach. The relationship between these different semi-classical schemes is outlined in Appendix B.

By following a different sequence of canceling and linearizing in the phase difference, an alternative scheme known as the linearized approach to non-adiabatic dynamics in the mapping Hamiltonian formulation, or LAND-map, has been developed [15,16]. As outlined in Appendix B, this LAND-map approach results in a force (see Equation B5) that depends on the states that label the density matrix elements being propagated rather than the mean force of Equation (9) that arises in the present PLDM approach. The linearized approximation within the LAND-map formulation must break down for longer time propagation but it can been used as a short time approximation that can be iterated yielding a "surface hopping" (SH)-like version of the approach known as Iterative Linearized Density Matrix (ILDM) propagation (see the Appendix for details) that can in principle be applied for accurate longer time propagation. This approach has been tested for various model quantum dynamical problems [26,27]. While ILDM uses a surface hopping like linearized expression as a short time approximation that is iterated to treat longer times, its convergence with large numbers of iterations can be problematic. The LAND-map approach [15,16] uses this same linearized approximation but without iteration. LAND-map has improved statistical convergence over the ILDM propagation approach but the linearized propagator underlying these methods is generally only reliable for short times and a balance between many iterations and statistical convergence must be considered. The mean trajectory linearized approximation underlying the PLDM scheme developed here, however, seems to be generally accurate for much longer times as demonstrated in the example applications presented below. The PLDM approach thus offers a significant improvement in statistical convergence while preserving high accuracy, even at long times.

3. Results

In this section, we present the results of calculations using the approach outlined above to compute different properties for a variety of model problems that provide stringent tests of the approximations underlying the method. Thus, results obtained for both electronic and nuclear properties computed with the PLDM approach are compared with exact benchmark calculations and results from other approximate theoretical approaches to explore the reliability and relative efficiency of these various calculations.

The first series of models treat one dimensional anharmonic molecular vibration and dissociation over a number of non-adiabatically coupled electronic surfaces described by a series of displaced and coupled Morse potentials. At low energies where the trajectories oscillate over the coupled surfaces and distribute their population amongst the different electronic states we demonstrate that the PLDM approach effectively solves the inverting potential problem of the original mapping Hamiltonian model [10,28], while at higher energies we show for similar models of molecular photodissociation on multiple surfaces [11,15,26] that the PLDM approach gives accurate, stable positive definite branching probabilities unlike the linearized semi-classical initial value representation (LSC-IVR) approach that can give unphysical negative populations when used to implement the mapping Hamiltonian formulation of the non-adiabatic dynamics problem.

The applicability of the PLDM approach for treating more complex non-adiabatic intramolecular vibrational dynamics such as in the regions of conical intersections is explored in a three-mode model of the vibrational dynamics in the conical intersection between the S_1 and S_2 states of pyrazine where results are compared with the time dependent self-consistent field (TDSCF) approach and quasi-classical mapping Hamiltonian (QC-map) methods, and exact multi-configuration time dependent Hartree (MCTDH) calculations. Despite the fact that the QC-map approach incorporates zero point energy corrections [13,25] we find that it gives unphysical negative adiabatic populations. The PLDM and TDSCF approaches do not suffer from this problem and can reproduce much of the qualitative behavior observed in the exact results for this model. Finally, we explore the conical intersection dynamics in a model *cis-trans* photoisomerization reaction [73–76], and study the dependence of the results on the initial torsional angle distribution.

Next we explore the performance of the approach for a condensed phase application involving a multi-state model of the dissipative quantum dynamics of excitation energy transfer in the Fenna–Mathews–Olsen (FMO) photosynthetic light harvesting complex where we show that the approach can capture both short time coherent dynamics and the thermal equilibration at longer times [12,27]. Comparison with exact results demonstrate that the approach is superior to alternative trajectory based, mixed quantum-classical methods, and that the approach is extremely efficient, giving results comparable to exact calculation with a small fraction of the computational effort.

3.1. *Low dimensional multi-state models*

3.1.1. *Coupled Morse potential models*

First, we focus on a one dimensional multi-state problem involving motion over a set of coupled electronic surfaces modeled by strongly anharmonic Morse potentials where each surface gives rise to a state dependent infinite repulsive wall at short bond-lengths. This is a classic situation for modeling non-adiabatic molecular photodissociation and vibrational dynamics leading to population redistribution over different electronic states as can occur in intersystem crossing processes. The potential inversion problem outlined above is particularly acute for these types of model multi-state processes. In previous work [10,28], Bonella and Coker showed that even for a single-state Morse potential with an initial incoming wave packet moving toward the infinite potential wall [10], the original mapping Hamiltonian, unless special problem dependent measures are taken, will indeed give unstable trajectories running on the inverse potential that can dominate the semi-classical trajectory ensemble resulting in noisy, highly-oscillatory, non-physical wave packets [10]. Here, we use the PLDM approach to describe strongly anharmonic motion over a set of coupled Morse surfaces [15,28], with Hamiltonian of the form:

$$\begin{aligned} H_{\lambda\lambda}(R) &= D_\lambda(1 - e^{-a_\lambda(R-b_\lambda)})^2 + E_\lambda \\ H_{\lambda\beta}(R) &= A_{\lambda\beta}e^{-c_{\lambda\beta}(R-d_{\lambda\beta})^2} \end{aligned} \tag{11}$$

with $D_1 = 0.0278$, $a_1 = 0.675$, $b_1 = 1.890$, $E_1 = 0$ and $D_2 = 0.01025$, $a_2 = 0.453$, $b_2 = 3.212$ and $E_2 = 0.0038$. Here, we work in atomic units and consider a proton mass moving over the coupled surfaces as displayed in the left panel of Figure 1. According to the linearization approach (see the results under Equation 9) the trajectory ensemble initial conditions must be sampled from the Wigner transform of the initial nuclear density *e.g.*, $\rho_{i,i}(R, R', t = 0) = \langle R|\chi\rangle\langle\chi|R'\rangle$ on electronic surface i. In these calculations we assume an initial Gaussian wave packet of the form:

$$\chi(R) = \left(\frac{2\alpha}{\pi}\right)^{1/4} e^{-\frac{\alpha}{2}(R-R_0)^2 + \frac{i}{\hbar}P_0(R-R_0)} \tag{12}$$

with $\alpha = 1$, $R_0 = 4$, and $P_0 = 0$, prepared on the initially excited potential surface 1, as presented in the left panel in Figure 1. With this particular initial condition, the problem is highly non-adiabatic since the wave packet travels back and forth through the coupling region many times. Also, the classical turning points of the motion on the different surfaces are well up on the inner walls so the original semi-classical implementation of the mapping Hamiltonian dynamics will generate trajectories running on a highly unphysical inverse potential in this region. The effects of these trajectories should in fact cancel each other out through interference of phase factors in a converged computation but achieving convergence in this situation for the semi-classical implementation can be very difficult.

The results of our PLDM calculations for this model are presented in the right panel of Figure 1 where we compare the time dependence of the expectation value of the population difference operator $\langle\hat{\sigma}_z\rangle(t) = \int dR[\rho_{11}(R, R, t) - \rho_{22}(R, R, t)]$ computed with the PLDM approach, the LAND-map approximation, and exact results obtained from fast Fourier transform split operator propagation. The LAND-map calculations give reasonable results only at short times as they assume that the dynamics proceeds on a single diabatic surface. The mean surface propagation underlying the PLDM approach, however, gives a reliable, semi-quantitative description of the dynamics out to much longer times, accurately capturing the high frequency oscillations corresponding to non-adiabatic dynamics between diabatic states 1 and 2, as well as the low frequency modulation associated with the nuclear motion over the coupled surfaces.

Next, we explore the reliability of different trajectory based methods for treating excited state dissociative dynamics using various three-coupled Morse potential surface models of non-adiabatic photodissociation dynamics [11,26]. The diabatic potentials and the couplings for the different models are presented in the left panels of Figure 2. In each case an initial wave packet with the same form as Equation (12) is prepared on diabatic state 1, and centered at the location indicated by the red arrow. The wave packet is given initial momentum $P_0 = 0$ to mimic a Franck–Condon excitation from some lower lying ground electronic state into the excited state manifold of the three coupled electronic states in which subsequent

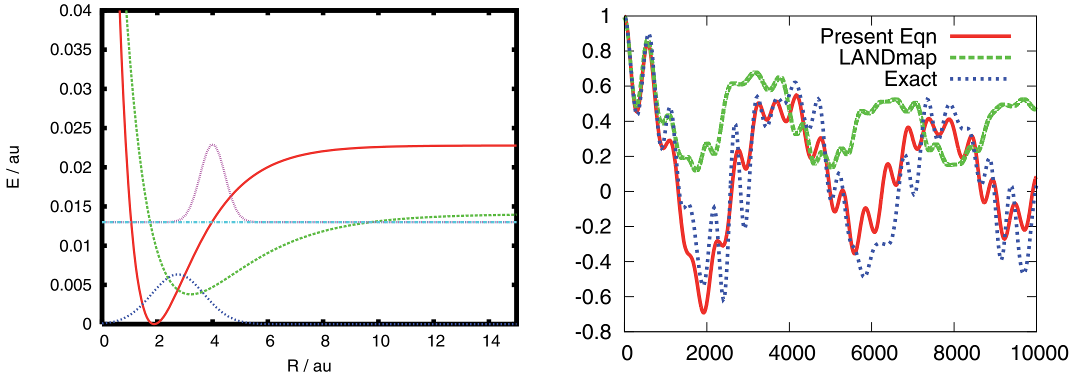

Figure 1. Left panel: Coupled Morse model potential surfaces: Red and green curves give the internuclear separation dependence of diagonal Morse potential surfaces for diabatic electronic states 1 and 2, and the blue Gaussian curve centered at the crossing point of the Morse potentials gives the bond-length dependence of the off-diagonal electronic coupling between these states [28,43]. The initial wave packet density (magenta Gaussian centered at 4 au) is also displayed. Right panel: $\langle \hat{\sigma}_z \rangle$ versus time (in au) computed using PLDM propagation (solid red curve), the LAND-map results (green dash curve), and exact results obtained with FFT split operator propagation (blue dotted curve).

non-adiabatic molecular photodissociation takes place. The parameters for the potentials and the initial wave packet can be found in Ref. [11].

By initially preparing the system in a wave packet centered high on the repulsive wall of a single excited state potential the packet should rapidly move out from this region and dissociate thus avoiding the inverting potential problems with the standard SC-IVR mapping Hamiltonian implementation. Despite these more favorable conditions for the standard implementation, earlier work using the SC-IVR approach for these problems [11] reported that the "barrier-like motion" still persists and generates approximately 1% problematic trajectories that have unphysically large prefactors ($\sim 10^8$) that represent dominant noise and have to be discarded from the ensemble to extract any useful signal. Moreover, the results obtained with these methods must be renormalized due to population leakage arising from the need to discard highly unstable trajectories. The renormalized SC-IVR results, however, agree well with the exact results once filtered in this way [11].

The right panel in Figure 2 compares exact calculations of the populations for different three-state dissociative models with results computed with the PLDM approach (Present), and the linearized approximate theory (LSC-IVR). For the model reported in the middle panels we see that the initial wave packet prepared in the strongly repulsive region on surface 1 very rapidly passes through the two closely spaced coupling regions and gives results that are in reasonable agreement with exact results and those of the PLDM calculations. This observation is consistent with the suggestion that moving rapidly to dissociation avoids problems with motion on the inverted potential. In the upper and bottom panels, on the other hand, we see that when the LSC-IVR approach moves more slowly through coupling regions difficulties analogous to the inverting potential problem cause serious inaccuracy in the LSC-IVR calculations. The case presented in the upper panel shows an unphysical situation where one of the populations actually goes negative with the LSC-IVR implementation due to the term $\rho_{ii}(t) \sim \left(p_i^2 + q_i^2 - \frac{1}{2}\right)$, while the lower panel shows that the approach can yield a highly inaccurate representation of the dynamics in the case of slower passage through regions of stronger coupling. Generally, however, we find that across a wide range of parameters for this model non-adiabatic photodissociation problem the present PLDM propagation approach captures the population relaxation dynamics quite accurately and our approach that employs the classical mapping Hamiltonian of the model [10,15,28] never suffers from problems related to potential inversion [11].

We should mention that for the nuclear DOF, the distribution of coordinates [49] or momenta [18] generated by the LSC-IVR approach must lose accuracy in representing the quantum mechanical features associated with the branching between different alternative surfaces due to the "mean surface" Ehrenfest-like forces employed with the approach. In contrast the Forward Backward IVR (FB-IVR) can capture this behavior accurately [18,49,50] and the approach can be implemented efficiently. With the current PLDM propagation approach, a mean surface type force is

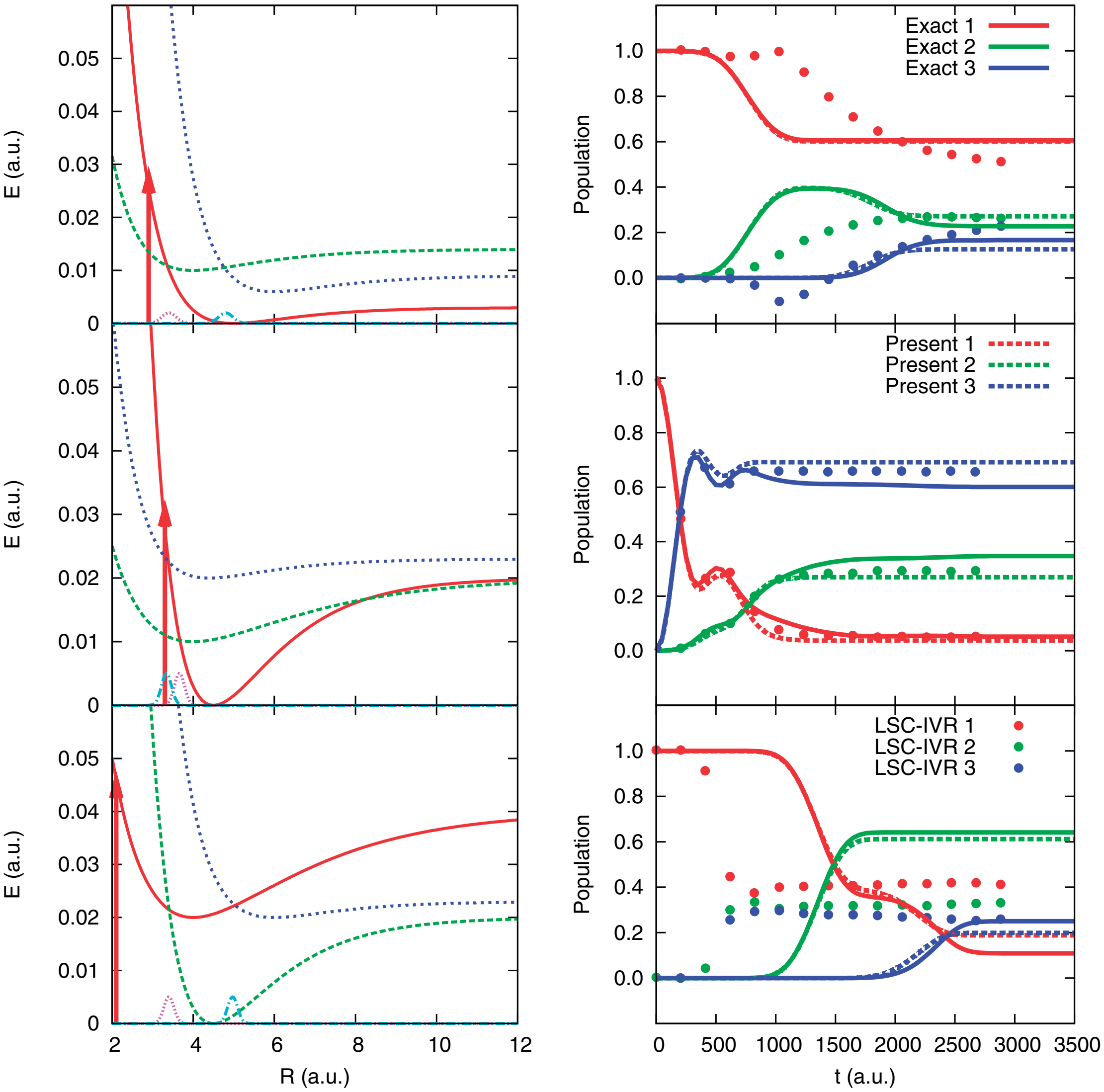

Figure 2. Results for various multiple Morse curve potential manifolds. The left panel shows model potentials and couplings [11] that are typical of non-adiabatic molecular photoexcitation and subsequent dissociation. Arrows indicate initial positions of nuclear wave packets. The right panels show evolution of diabatic state populations color coded to match the potential curves. Solid curves are exact populations (calculated with FFT split operator propagation), dashed curves give populations computed using PLDM propagation and filled circles give results obtained with LSC-IVR.

used to drive the nuclear DOF, so although it seems to be an optimal mean surface approach it must suffer from an inability to capture the back reaction effects of the non-adiabatic branching on the nuclear DOF.

This is a well-known disadvantage of ‘‘Ehrenfest mean field type dynamics’’ compared to, for example, surface hopping dynamics [2,3,64], that can capture different nuclear alternatives by stochastic hops between different surfaces. A surface hopping version of the LAND-map approach, known as iterative linearized density matrix (ILDM) propagation (see Appendix B and reference [26]) can capture these branching processes. Exploratory studies of the iterative implementation of the present PLDM propagation approach suggest that this may be a productive way to combine the superior convergence properties of the PLDM approach with the more accurate surface hopping characteristics of ILDM propagation.

3.1.2. *Model conical intersection dynamics in photoexcited pyrazine*

In this section, we extend our exploration of the PLDM approach for multi-surface non-adiabatic quantum dynamics beyond the limits of a single nuclear DOF and use the approach to study a simplified model of the S_1–S_2 conical intersection dynamics in pyrazine [13,30,42], which is a well studied benchmark system for exploring the reliability of semi-classical and other approximate theories [42] for higher dimensional non-adiabatic problems. Here, we adopt a two-state, three-mode pyrazine model from Ref. [13,14]. The model Hamiltonian is:

$$\hat{H}=\sum_{\beta=S_1}^{S_2}\left[E_\beta+\sum_{j=1,6a,10a}\frac{1}{2}\left[P_j^2+\omega_j^2R_j^2\right]+c_j^\beta R_j\right]|\beta\rangle\langle\beta| + \sum_{j=1,6a,10a}\lambda_jR_j[|S_1\rangle\langle S_2|+|S_2\rangle\langle S_1|] \tag{13}$$

where $E_{S_1}=3.94\,\text{eV}$, $E_{S_2}=4.84\,\text{eV}$; $\omega_1=0.126\,\text{eV}$, $\omega_{6a}=0.074\,\text{eV}$, $\omega_{10a}=0.118\,\text{eV}$, $c_1^{S_1}=0.037\,\text{eV}$, $c_1^{S_1}=-0.037\,\text{eV}$, $c_{6a}^{S_1}=-0.105\,\text{eV}$, $c_{6a}^{S_2}=0.105\,\text{eV}$, $\lambda_{10a}=0.262\,\text{eV}$, and $\lambda_j=0$ for all other system–bath bilinear coupling constants.

This model has a similar form to the system–bath Hamiltonian in Equation (15) below, which we use to describe excitation energy transfer in model photosynthetic systems. There are however two major differences: (1) In the excitation energy transfer model of Section 3.2.1 each state, involving the excitation localized in a different region of space, has its own independent bath, whereas in the pyrazine model outlined here, the bath oscillators are the vibrational modes of the molecule and are thus the same for each quantum state; they may just couple with different strengths. (2) The other important difference concerns the off-diagonal electronic coupling, which in the case of the excitation energy transfer model considered in Section 3.2.1, is a constant independent of bath coordinates. In contrast, for the conical intersection problem considered here, the electronic coupling between the S_1 and S_2 states depends linearly on the bath coordinate R_{10a}. We have recently explored the influence of such bath dependent electronic coupling terms on the excitation energy transfer in a variety of generalized models for protein-pigment photosynthetic light harvesting systems [40].

In Figure 3, left panels (A) and (B), we present a comparison of the diabatic and adiabatic population computed with PLDM propagation, the time dependent self-consistent field (TDSCF) method [14], the quasi-classical mapping equation (which is the same as the LSC-IVR approach with full zero point energy correction [13]), and the exact quantum results for this model. The PLDM propagation results are found to be close, but not identical to the TDSCF results, and reproduce the basic dynamical features seen in the full quantum calculations though the amplitudes of the oscillatory features in full quantum results are more pronounced, for example, for the diabatic populations presented in Figure 3 (A). This suggests that for this model the PLDM approach has similar shortcomings in treating zero point energy flow between the quantum and classical degrees of freedom to the TDSCF approach.

The adiabatic populations computed with the PLDM and TDSCF methods, however, tend to different long time asymptotic values than the full quantum results suggesting that the wave packet propagated with these mean field methods give different quality results depending on the representation employed. Despite these problems, the PLDM approach and the TDSCF method both give positive definite populations in contrast to the situation observed, for example, with the adiabatic populations obtained with the quasi-classical mapping Hamiltonian approach, which behaves similarly to the LSC-IVR implementation of the mapping Hamiltonian and can give unphysical negative populations.

The right panels of Figure 3 compare trajectories of average positions and momenta of various nuclear modes computed with the different methods. For this multi-dimensional conical intersection model we see that both the PLDM and TDSCF approaches reproduce the exact results with high fidelity, though the phase of the oscillations begins to walk off by about 350 fs. The QC-mapping equation approach gives slightly better agreement with the full quantum results for the first couple of periods but then approaches different asymptotic values and gives incorrect phases for longer times. These results mirror the situation observed with the diabatic populations in the left panel (A).

3.1.3. *Model conical intersection dynamics in photoisomerization*

The final intramolecular non-adiabatic dynamical model we consider here explores the conical intersection dynamics associated with a photoisomerization reaction. The two-state, three-mode model of *cis*-*trans* photoisomerization [73–76] is described by the following Hamiltonian:

$$H=\frac{L_\varphi^2}{2I}+\sum_{j=c,t}\frac{\omega_j}{2}(p_j^2+q_j^2) + \begin{bmatrix} \epsilon_0+\frac{1}{2}W_0(1-\cos\varphi) & \lambda q_c \\ \lambda q_c & \epsilon_1+\frac{1}{2}W_1(1-\cos\varphi)+\kappa q_t \end{bmatrix} \tag{14}$$

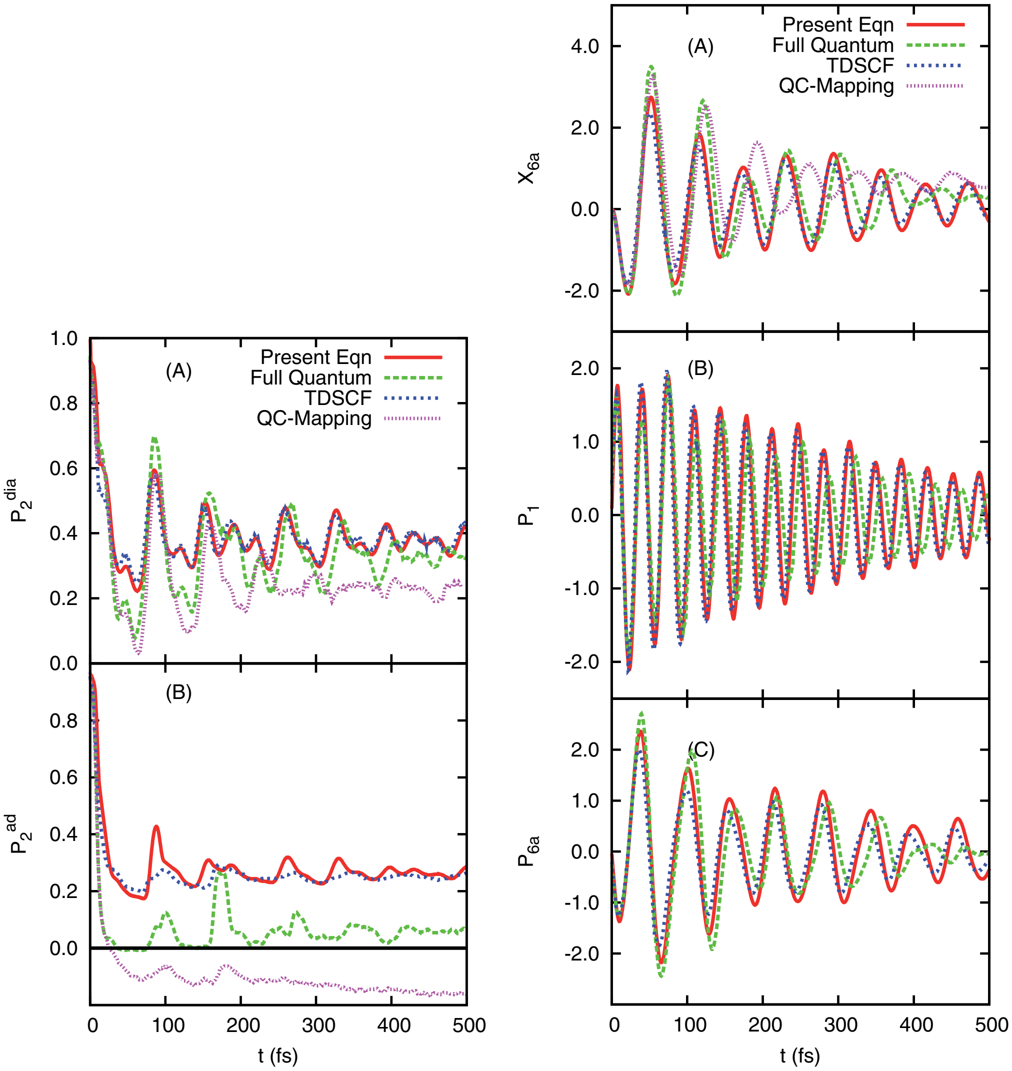

Figure 3. Three-mode pyrazine model. Left panels: comparison with PLDM (red solid), exact results (green long dash), TDSCF (blue short dash), and the quasi-classical mapping expression (magenta dotted) for (A) diabatic and (B) adiabatic populations. The exact, TDSCF and QC-mapping result are reproduced from Refs. [13,14]. Right panels: comparison of mean position and momentum of various bath modes computed with different methods. The line types are the same as for the left panels.

where φ, q_c, q_t are the torsional, coupling and tuning modes respectively, and $L_\varphi = -i\frac{\partial}{\partial\varphi}$ is the angular momentum for the torsional mode. In this Hamiltonian, all the nuclear DOF are unitless and the parameters (in eV) are [73–76]: $\omega_t = 0.1$, $\kappa = 0.15$, $\omega_c = 0.085$, $\lambda = 0.17$, $I^{-1} = 5.5 \times 10^{-4}$, $\varepsilon_0 = -2.5$, $\varepsilon_1 = 0$, $W_0 = 2.25$, $W_1 = -2.25$.

In Figure 4, results from the PLDM dynamics approach are compared with those from exact quantum calculations and QC-mapping Hamiltonian dynamics ($\gamma = 0.5$). In all these calculations the system is initially prepared in the $|S_1\rangle$ electronic excited state and different initial conditions for the torsional mode are employed; in particular we consider three different energy regimes: (a) $E > 0$: an initial wave packet centered at $\varphi = 0$ with an additional kinetic energy of $T = 0.15\,\text{eV}$, (b) $E = 0$: symmetric preparation of the system at $\varphi = 0$ without initial kinetic energy, and (c) $E < 0$: an initial wave packet centered at $\varphi = 0.4\pi$ with a kinetic energy of $T = 0.15\,\text{eV}$. Both the electronic diabatic state population $P_{|S_1\rangle} = |S_1\rangle\langle S_1|$ and the probability of the system to be found near where it starts in the *cis* configuration $P_{cis} = 1\text{-}\Theta(|\varphi| - \pi/2)$, regardless of electronic state, are present in the top and bottom panels of Figure 4 respectively. In all cases, our PLDM results are found to agree closely with the results of the QC-mapping ($\gamma = 0.5$) calculations. The agreement with the full quantum result is better for the cases when $E = 0$ or $E > 0$.

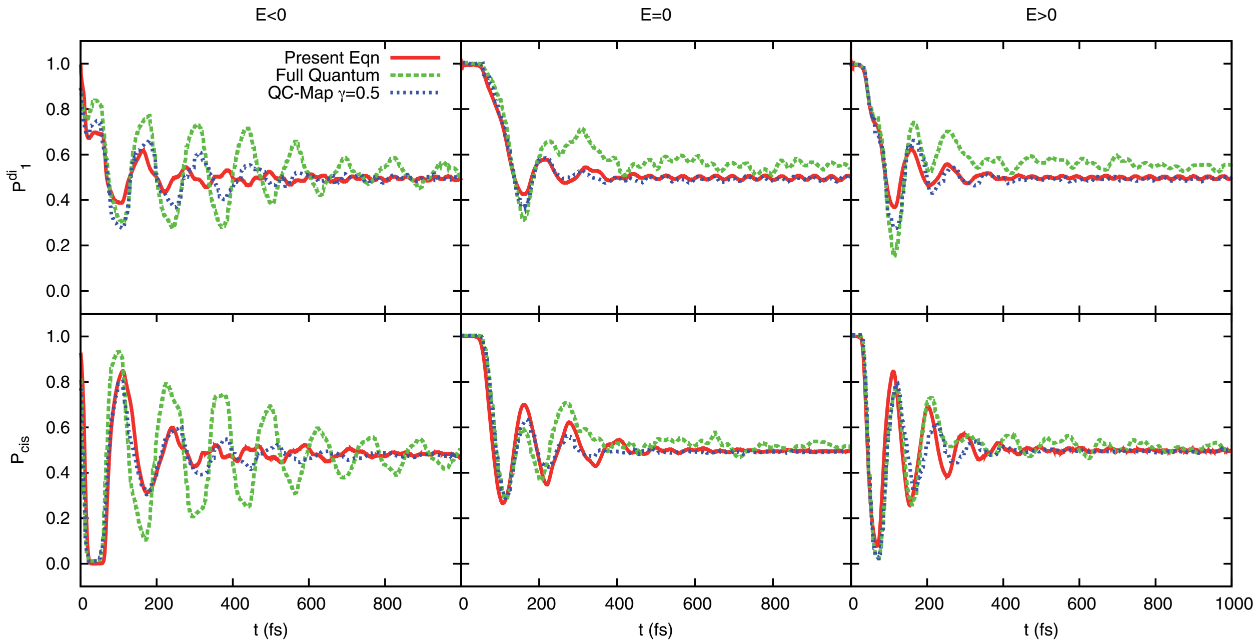

Figure 4. Conical intersection dynamics in a two-state, three-mode photoisomerization model. In all panels results for the PLDM dynamics (present approach) are given by the solid red curve, full quantum dynamics results (obtained from reference [73]) are presented as the dash green curves, and the results of quasi-classical mapping dynamics (with the zero point energy correction parameter set at $\gamma = 0.5$) are presented as the dotted blue curves. The top panels give electronic diabatic state populations in the S_1 state as a function of time obtained by averaging the state projection operator $P_{|S_1\rangle} = |S_1\rangle\langle S_1|$. The bottom panels give the probability that the system stays in the initial *cis* configuration obtained by averaging the angle projection operator $P_{cis} = 1\text{-}\Theta(|\varphi| - \pi/2)$. Different initial conditions for the torsional angle distribution sampling different energies are explored in the various columns (see text or detail).

Generally we see that for this photoisomerization model the approximate mean field methods give coherent oscillatory features that wash out too quickly compared with the longer lived, larger amplitude oscillatory features found in the full quantum results. This is largely due to the quasi-classical mean field treatment of the nuclear DOF with these approximate methods. Nevertheless the qualitative behavior is reasonably well captured by such approaches at higher energies. A detailed analysis of the oscillatory behavior observed in different regimes is presented in Ref. [73].

3.2. *High dimensional multi-state models of condensed phase systems*

Understanding how quantum effects such as coherence, dispersion, and tunneling survive in many-body condensed phase systems is a considerable challenge to modern theory. Many important properties such as excitation energy transfer, electron transport, and other non-equilibrium properties of nanostructured materials may depend critically on the survival of these quantum effects so methods that can reliably handle quantum behavior in large-scale systems such as the PLDM propagation approach and other approximate methods explored in this paper are of great practical importance. Thus, as demonstrated in the low dimensional model problems of the previous sections, while these methods often provide qualitatively reliable treatment of quantum effects in such a few DOF systems, their ability to treat such phenomena in large-scale systems where application of exact quantum dynamics methods is intractable often provides the only way forward. With this view in mind, in the final two subsections of results we explore several model condensed phase systems where benchmark calculations can be run and demonstrate that the PLDM propagation approach offers a highly efficient and extremely reliable way of treating such challenging high dimensional problems. The benchmark models make assumptions about the Hamiltonian (*e.g.*, a bilinearly coupled harmonic bath with a simplified spectral density). Such approximations are necessary so that exact benchmark calculations for these high dimensional complex problems can be conducted; however, the PLDM propagation approach does not require such simplifications to the Hamiltonian and once the reliability of the approach has been demonstrated in these benchmark studies it can be readily applied beyond the limits of these simple models.

3.2.1. *Multiple interacting quantum states coupled to independent baths: Excitation energy transfer in light harvesting*

Recently there has been considerable interest in the experimental observation of long lived quantum coherent dynamics in nanostructured materials composed of excitable chromophores embedded in polymers [55–58]. Understanding the origins and significance of this coherence for excitation energy transfer and transformation in photosynthetic light harvesting, with applications to design of new materials for solar energy, has attracted considerable interest from theory and experimental groups alike. These systems operate in regimes where the approximations underlying many of the standard approaches like Redfield theory and Forster resonance energy transfer (FRET) theory breakdown [41]. Thus new theoretical methods that can handle simultaneously strong system–bath and electronic coupling, non-Markovian spectral densities and dynamics beyond the secular approximation where populations and coherence terms in the evolution equations strongly influence one another are of great importance. Below we show that the PLDM propagation approach developed in this paper provides a highly accurate, and computationally efficient method for studying both the quantum coherent dynamics and long time evolution to thermal equilibrium in these technologically interesting quantum dissipative excitation energy transfer systems.

The model that has become the paradigm for treating such systems, which captures the basic physics of this dissipative multi-chromophore excitation energy transfer problem, involves a set of electronically coupled two-level systems that each interact with its own independent bath of harmonic oscillators. The Hamiltonian for this model thus has the following form:

$$\hat{H} = \sum_{\alpha=1}^{N_{state}} \epsilon_\alpha |\alpha\rangle\langle\alpha| + \sum_{\alpha\neq\beta}^{N_{state}} \Delta_{\alpha,\beta}[|\alpha\rangle\langle\beta| + |\beta\rangle\langle\alpha|] + \sum_{\alpha=1}^{N_{state}} \sum_{i=1}^{n^{(\alpha)}} \left\{ \frac{1}{2}\left[P_i^{(\alpha)2} + \omega_i^{(\alpha)2} R_i^{(\alpha)2} \right] + c_i^{(\alpha)} R_i^{(\alpha)} \right\} |\alpha\rangle\langle\alpha| \tag{15}$$

and typical parameterizations for realistic models of photosynthetic light harvesting systems can be found in the references [12,27,31,41]. For the particular model considered here the system–bath interactions are determined by the Debye spectral density, $J^{(\alpha)}(\omega) = 2\lambda^{(\alpha)}\omega\tau_c^{(\alpha)}/(1+\omega^2\tau_c^{(\alpha)2})$, and a modified sampling approach is employed.^{2} With this model there are different independent baths of oscillators, each with, in principle, a different spectral density, $J^{(\alpha)}(\omega)$, labeled by state index, α.

Photosynthetic excitation energy transfer networks often include at least one pair of chromophores that are strongly electronically coupled forming a dimer, and excitation energy is observed to coherently oscillate between the two coupled states or "sites" of the dimer. In typical photosynthetic light harvesting networks these dimers are weakly electronically coupled to other monomer chromophores in the network so excitation energy in the dimer can be both dissipated to the local bath environment or transferred to these other chromophores. In this section we use typical parameters for such networks and explore the ability of various approximate quantum dynamics methods to capture the interplay between coherent energy transfer between the component chromophores in dimers, subsequent population transfer to monomers and dissipation of excitation energy from the chromophore network to the surrounding environment.

As a first example system we consider a simplified two-state model equivalent to the spin-boson model presented above but with physically reasonable parameters for photosynthetic systems [12,27,41]; in particular we choose the energy gap between the diabatic dimer states to be $(\epsilon_1 - \epsilon_2) = 100\,\mathrm{cm}^{-1}$, the electronic coupling is $\Delta_{1,2} = 100\,\mathrm{cm}^{-1}$, and the temperature is $T = 300\,\mathrm{K}$. The results reported in Figure 5 have the bath relaxation time $\tau_c = 100\,\mathrm{fs}$ and we have also studied the behavior of this system with a slower bath relaxation time ($\tau_c = 500\,\mathrm{fs}$) where non-Markovian effects are expected to play a significant role. The environment coupling strength or solvent reorganization energy, λ, was varied over a range of values: 2, 20, 100, and $500\,\mathrm{cm}^{-1}$. In Figure 5 populations obtained for the various approximate methods are compared with results of hierarchical coupled reduced master equation (HCRME) calculations [41], which, when the hierarchy can be converged, provide numerically exact results for this specific spectral density. In previous work on this model [27,41], with its realistic parameterization, it was demonstrated that the standard Redfield theory approach only gave reasonable results at the lowest values of friction and shortest bath relaxation times, otherwise the Redfield theory, based on a perturbative treatment of the bath interaction and the Markovian approximation, gives excessively rapid damping of the coherent oscillations, and too fast an approach to thermal equilibrium.

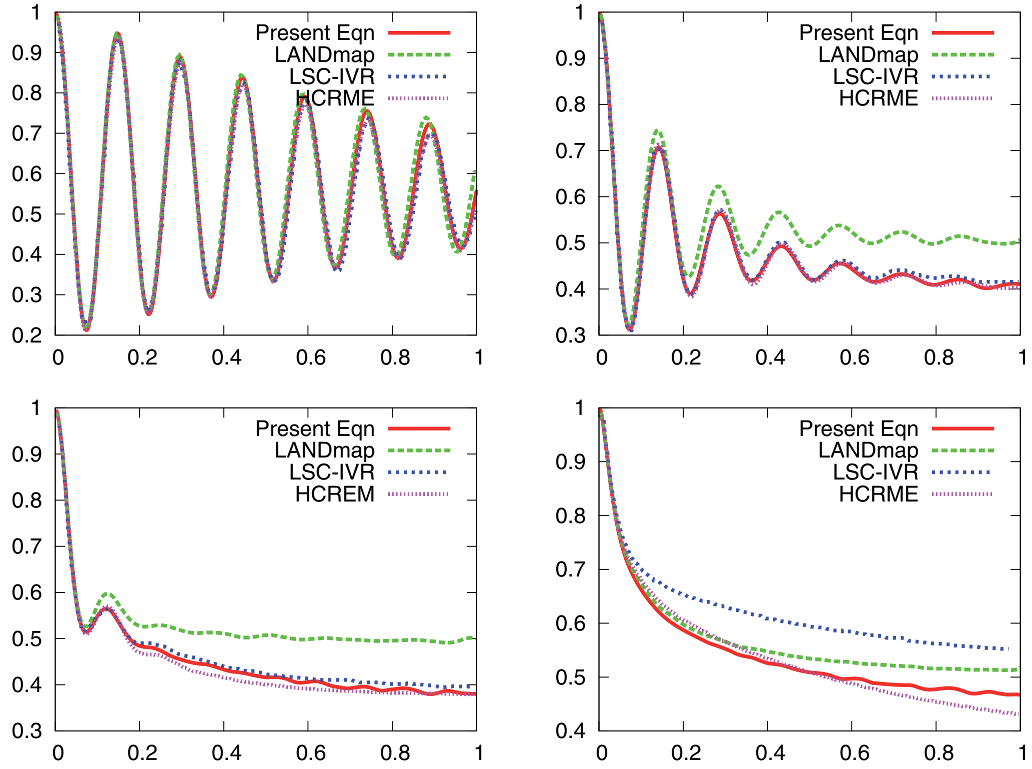

Figure 5. Population of site 1 as a function of time (in ps) for a two-state model [41]. The exciton state energy gap is $(\epsilon_1 - \epsilon_2) = 100\,\mathrm{cm}^{-1}$, the excitonic coupling is $\Delta_{1,2} = 100\,\mathrm{cm}^{-1}$, the temperature is $T = 300\,\mathrm{K}$, the characteristic time of the phonon bath is $\tau_c = 100\,\mathrm{fs}$, and the solvent reorganization energy is varies as $\lambda = 2\,\mathrm{cm}^{-1}$ (upper left), $\lambda = 20\,\mathrm{cm}^{-1}$ (upper right), $\lambda = 100\,\mathrm{cm}^{-1}$ (lower left), and $\lambda = 500\,\mathrm{cm}^{-1}$ (lower right). Both the present model and the LAND-map results are calculated using the non-adiabatic dynamics theory outlined in this paper. Linearized semi-classical initial value representation (LSC-IVR) theory results are taken from reference [12]. Exact results using the hierarchical coupled reduced master equation (HCRME) approach are taken from reference [41].

For the linearized semi-classical approaches, however, the general trends observed in these two-state system results, as discussed in earlier work [27], are that LAND-map and LSC-IVR provide reasonable qualitative descriptions of how the strong amplitude of the short time coherent oscillations damp out as the system approaches its long time steady state behavior. The long time equilibrium values for these different approximate methods, however, approach different values. With the LAND-map approach, as outlined earlier, the equilibrium population always tends to infinite temperature result (0.5, for this two-level system). Similar problems with thermal equilibration have recently been reported using the Ehrenfest dynamics approach for this model [38]. The quality of the results for the LSC-IVR approach, however, seems to depend on the strength of coupling between the two-level system and its harmonic bath. For weak to intermediate system–bath coupling, λ, the LSC-IVR results are in excellent agreement with exact results for all times. For strong friction, however, the LSC-IVR results decay too slowly and seem to tend to the wrong equilibrium, as though the system is trapped in its starting state by the sluggish bath [68]. Generally we find that results from these approximate methods agree better with exact results when the bath relaxation time is longer; surprisingly these linearized semi-classical methods provide better results when non-Markovian memory effects are stronger [27].

The present PLDM propagation approach, however, is found to give near quantitative agreement with the exact HCRME results across the entire range of conditions studied in these model calculations. In previous work [27] we tested the ILDM propagation approach with this model and verified that, when we could get the calculations to converge, the results were in excellent agreement with those obtained from the exact HCRME approach. The problem with the ILDM propagation approach is that large trajectory ensembles, typically on the order of $\sim 10^7$ to 10^8 trajectories, are often required to provide converged results and this situation deteriorates at longer times and in certain parameter regimes [27]. These problems are completely solved with the present PLDM approach, which we find requires comparatively modest ensembles, typically on the order of $\sim 10^4$ trajectories for these types of problems, and propagation to significantly longer times in these types of model systems is not prohibitive. Finally, it is important to note that, unlike the HCRME approach, the semi-classical methods do not use analytical results dependent on the form of the spectral density in their implementation and can thus be applied to general arbitrary model spectral densities. Given the accuracy, and stability for long time propagation, of the PLDM approach and its applicability to general model spectral densities, this new method offers an extremely powerful theoretical tool for treating realistic large scale models of excitation energy transfer.

To demonstrate these important properties of the PLDM approach, finally in this section, we present results for a multi-state version of the system-independent bath model defined by the Hamiltonian in Equation (15), which has been parameterized, and used in many recent theoretical studies [12,27,31,35,37,59,60] of the $N_{state} = 7$ model of the Fenna–Matthews–Olsen (FMO) photosynthetic light harvesting antenna complex. Most of the model studies of this system to date assume identical independent spectral densities for each chromophore, and the Debye or exponential cutoff models are popular.

When applied to this multi-state model the LSC-IVR approach actually gives unphysical negative populations for some of the states [12] for the reasons discussed in Section 3.1.1. Like the LAND-map approach [27], the mixed quantum-classical Liouville–Poisson bracket mapping equation (PEMB) approach [35] captures the short time coherent behavior of this model but fails to reproduce accurate relaxation to a proper Boltzmann equilibrium distribution. A number of recently devised approximate reduced master equation approaches such as the non-Markovian quantum jump (NMQJ) with time convolutionless master equation [31], the non-Markovian quantum state diffusion (NMQSD) equation [34], and the generalized Bloch–Redfield (GBR) model with the non-interacting blip approximation (NIBA) [61], however, give reliable results for this and related models. Other, less sophisticated reduced master equation approaches, either reproduce the short time coherent dynamics and not the long time thermal equilibrium or *vice versa*. Thus, for example, as mentioned above the standard Redfield equation fails to capture the short time coherent dynamics reliably, but recovers the long time thermal equilibrium populations. In contrast, the stochastic Liouville equation (SLE) [37] or Ehrenfest dynamics approach [38] fails to give the correct long time thermal equilibrium limit, but gives an accurate account of the coherent short time dynamics.

In earlier work [17,27] we used this FMO model system as a benchmark and in detailed comparisons with the results of exact HCRME [41,59] and the rescaled version of the theory [60] we showed that our ILDM approach and the highly efficient PLDM approximate version [17] gave quantitatively accurate results for all times. In recent work [62] we have converged calculations with the PLDM approach for very long times, *e.g.*, we have been able to follow the relaxation to thermal equilibrium of the weakly coupled inter-complex energy transfer between the CP47/CP43 light harvesting antenna complexes and the reaction center (RC) in photosystem II requiring reliable quantum dynamical treatment out to more than 50 ps.

In Figure 6, the excitation energy transfer dynamics in the seven-state FMO model at elevated temperatures ($T = 300\,\mathrm{K}$) is presented. These results obtained with the PLDM approach are graphically indistinguishable from the results of HCRME calculations [59,60] and show short time coherent population beating between strongly coupled dimers in the system and long time thermal equilibration. Results of comparable accuracy for this system have recently been obtained using a hybrid NIBA–Ehrenfest approach [63]. The path towards equilibrium from initial site 6 (right panels) involves excitation energy transfer between two coupled dimers: chromophores 6-5, and 4-7 and the transient coherent quantum beating of these coupled states is evident in the population oscillations of these chromophore dimers. The dynamics initiated in site 1 (left panels), on the other hand, involves a single coupled dimer that is weakly coupled to the other chromophores in the network. The upper and lower panels give results that explore the influence of bath relaxation time on the lifetime of the quantum coherent population beating.

4. Concluding remarks

In this paper we have shown that the partial linearized density matrix (PLDM) propagation approach gives a new "mean field" version of non-adiabatic quantum dynamics that out-performs many other such approaches in terms of both accuracy and numerical efficiency. Being a mean field approach, however, the new method cannot accurately account for the "back reaction" between the classical and quantum DOF that occurs, for example, when the quantum subsystem undergoes a transition. Nevertheless we find that the

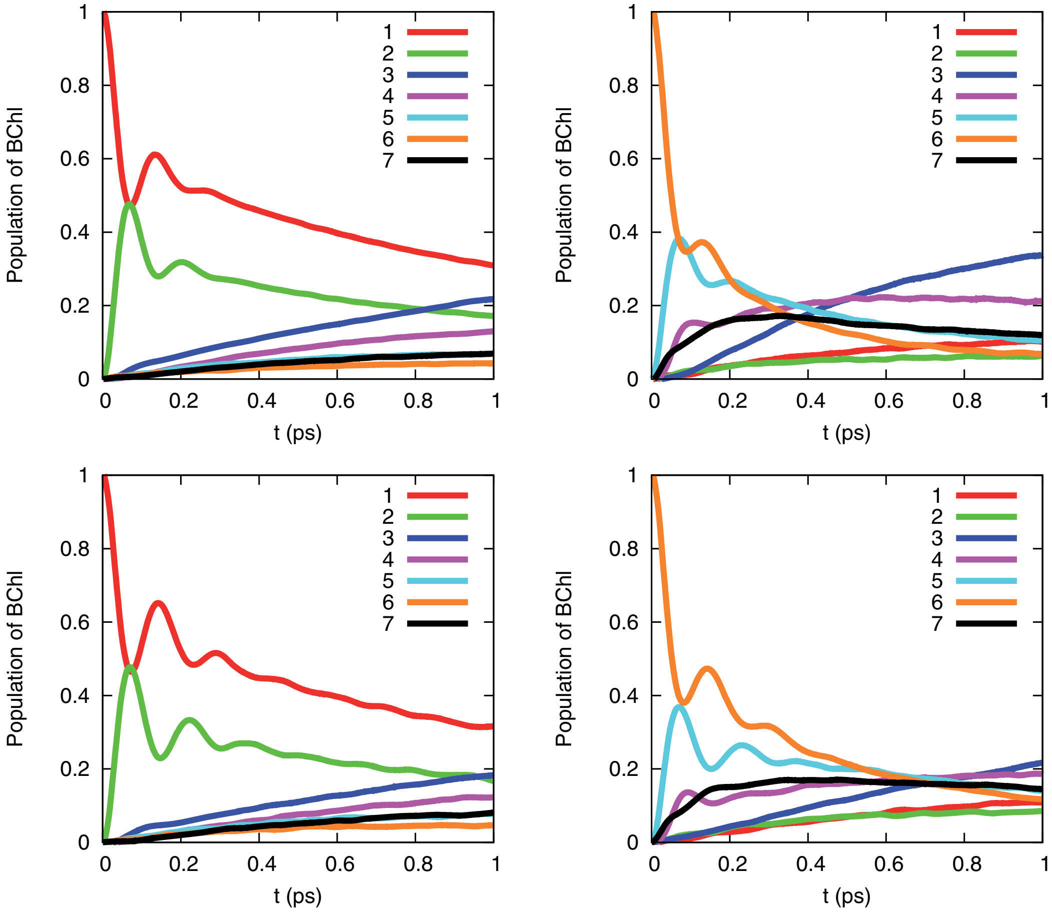

Figure 6. Population for the seven-state FMO model at 300 K with initial excitation at site 1 (left column) or site 6 (right column). The upper panels give results with the faster relaxation time $\tau_c = 50$ fs, and the bottom panels are computed with the slower relaxation time of $\tau_c = 166$ fs. These results are graphically indistinguishable from the exact results of HCRME [59] (not shown in the figure).

approach does seem to capture both short time coherent dynamics and long time thermal equilibration in the various model systems studied, unlike many other mean field like approaches.

We devised the PLDM approach with state independent mean field-like forces as a compromise to address statistical convergence issues with the iterative linearized density matrix (ILDM) propagation scheme that we developed in previous work. The ILDM approach is more like a surface hopping scheme that involves the short time propagation of the nuclear DOF on a single diabatic surface, representing the evolution of populations, or an off-diagonal "surface" representing the evolution of coherence terms in the density matrix. With the ILDM approach stochastic hops take the members of the ensemble between these different types of terms that all play a role in modeling various contributions to the evolution of the full system density matrix. Compared to ILDM, the present PLDM approach is more like a mean surface "Ehrenfest dynamics" approach, though it solves many difficulties with other related mean field approaches.

When wave packets emerge from non-adiabatic coupling regions, a mean field, Ehrenfest like approach must give that the system continues to evolve with a mean surface force and thus can never give the right nuclear dynamics, though as we have seen for various scattering models the PLDM approach does give very good results for electronic populations in such situations. Alternatively, the ILDM surface hopping-like method will give the correct description, due to the state dependent force that this approach employs. However, for describing other types of physical phenomena, for example, where the coupling is slowly varying or constant and can be finite for long times a "mean force" approach can provide a good description, while a SH approach like ILDM will be constantly hopping between forces describing the different states that are involved in the dynamics and this behavior can cause serious convergence problems. This is precisely the reason our PLDM calculations perform so well for the multi-state system–bath interaction models that are widely used in modeling excitation energy transfer dynamics whereas our ILDM calculations on these models can only give converged results for relatively short times.

One can imagine merging the advantages of these two types of approaches to give an *ad hoc* propagation scheme that employs a mean field force at the coupling region, and single surface force beyond [51,52]. It may be possible to put such a scheme on a more rigorous footing by grafting the PLDM propagator and the iterative scheme together [77] based on a rigorous semiclassical path integral like approach similar to ILDM but with improved convergence properties.

Acknowledgements

We gratefully acknowledge support for this research from the National Science Foundation under grant CHE-0911635 and support from Science Foundation Ireland under Grant Number 10/IN.1/I3033. DFC acknowledges the support of his Stokes Professorship in Nanobiophysics from Science Foundation Ireland. PH wants to thank Guohua Tao and Jian Liu who, respectively, pointed out the importance of using the mapping Hamiltonian force to get the correct asymptotic behavior and the ‘‘running on the inverse potential’’ problem associated with the original mapping Hamiltonian. We also acknowledge a grant of supercomputer time from Boston University's Office of Information Technology and Scientific Computing and Visualization. Finally, thanks Bill for your inspirational work over all these years.

Notes

1. The idea of focusing [15] replaces the sampling of the mapping variable initial conditions from $e^{-\frac{1}{2}\sum_\beta(q_{\beta 0}^2+p_{\beta 0}^2)}$ by approximating the integral over initial conditions using the steepest descent method giving a delta function initial condition sampling distribution $\delta(\{q_{n_0}^2+p_{n_0}^2\}-2)$.
2. If $J(\omega)=2\lambda\omega\tau_c/(1+\omega^2\tau_c^2)$ and also $J(\omega)=\frac{\pi}{2}\sum_j\frac{c_j^2}{M_j\omega_j}\times\delta(\omega-\omega_j)$, with the density of states (DOS) $\rho(\omega)=\delta(\omega-\omega_j)$, we get $c_j^2=\frac{2}{\pi}\omega_j\frac{J(\omega_j)}{\rho(\omega_j)}$. By choosing $\rho(\omega)=a\frac{J(\omega)}{\omega}$, together with $\int_0^{\omega_j}\rho(\omega)=j$ and $\int_0^{\omega_m}\rho(\omega)=N_b$ (where N_b is the total number of oscillators that correspond to the total DOS, and ω_m is the maximum frequency of the spectral density which is the numerical cutoff), we have $a=N_b/(2\lambda\tan^{-1}(\omega_m\tau_c))$, $c_j=2\sqrt{\lambda\tan^{-1}(\omega_m\tau_c)/\pi N_b\omega_j}$ and $\omega_j=\tan(j\ \tan^{-1}\times(\omega_m\tau_c)/N_b)/\tau_c$.

References

[1] P. Pechukas, Phys. Rev. **181**, 174 (1969).
[2] J.C. Tully, J. Chem. Phys. **93**, 1061 (1990).
[3] J.C. Tully, in *Classical and Quantum Dynamics in Condensed Phase Simulations*, edited by G. Ciccotti, B. Berne, and D. Coker (World Scientific, Dordrecht, 1998), p. 489.
[4] J. Bader and B. Berne, J. Chem. Phys. **100**, 8359 (1994).
[5] B. Berne, J. Bader and P. Hanggi, J. Chem. Phys. **104**, 1111 (1996).
[6] S. Egorov, E. Rabani and B. Berne, J. Phys. Chem. A **103**, 10978 (1999).
[7] H.D. Meyer and W.H. Miller, J. Chem. Phys. **70**, 3214 (1979).
[8] G. Stock and M. Thoss, Phys. Rev. Lett. **78**, 578 (1997).
[9] M. Thoss and G. Stock, Phys. Rev. A **59**, 64 (1999).
[10] S. Bonella and D.F. Coker, J. Chem. Phys. **114**, 7778 (2001).
[11] E.A. Coronado, J. Xing and W.H. Miller, Chem. Phys. Lett. **349**, 512 (2001).
[12] G. Tao and W.H. Miller, J. Phys. Chem. Lett. **1**, 891 (2010).
[13] U. Müller and G. Stock, J. Chem. Phys. **111**, 77 (1999).
[14] G. Stock and M. Thoss, in *Mixed quantum-classical description of the dynamics at conical intersections: Conical intersections*, edited by W. Domcke, D.R. Yarkony, and H. Köppel (World Scientific, Singapore, 2003).
[15] S. Bonella and D.F. Coker, J. Chem. Phys. **118**, 4370 (2003).
[16] S. Bonella and D.F. Coker, J. Chem. Phys. **122**, 194102 (2005).
[17] P. Huo and D.F. Coker, J. Chem. Phys. **135**, 201101 (2011).
[18] N. Ananth, C. Venkataraman and W.H. Miller, J. Chem. Phys. **127**, 084114 (2007).
[19] X. Sun, H. Wang and W.H. Miller, J. Chem. Phys. **109**, 7064 (1998).
[20] J.A. Poulsen, G. Nyman and P.J. Rossky, J. Chem. Phys. **119**, 12179 (2003).
[21] Q. Shi and E. Geva, J. Chem. Phys. **118**, 8173 (2003).
[22] J. Vanicek, Phys. Rev. E **70**, 055201(R) (2004).
[23] N. Ananth and T.F. Miller III, J. Chem. Phys. **133**, 234103 (2010).
[24] Z. Ma and D.F. Coker, J. Chem. Phys. **128**, 244108 (2008).
[25] U. Müller and G. Stock, J. Chem. Phys. **108**, 7516 (1998).
[26] E.R. Dunkel, S. Bonella and D.F. Coker, J. Chem. Phys. **129**, 114106 (2008).
[27] P. Huo and D.F. Coker, J. Chem. Phys. **133**, 184108, (2010) (2010).
[28] S. Bonella and D.F. Coker, Chem. Phys. **268**, 189 (2001).
[29] G. Stock, J. Chem. Phys. **103**, 1561 (1995).
[30] G. Stock, J. Chem. Phys. **103**, 2888 (1995).

[31] R. Chakraborty, P. Rebentrost and A. Aspuru-Guzik, J. Chem. Phys. **131**, 184102 (2009).

[32] A. Ishizaki and G.R. Fleming, Proc. Natl. Acad. Sci. **106**, 17255 (2009).

[33] J. Zhu, S. Kais, P. Rebentrost and A. Aspuru-Guzik, J. Phys. Chem. B. **115**, 1531 (2011).

[34] G. Ritschel, J. Roden, W.T. Strunz, A. Aspuru-Guzik and A. Eisfeld, J. Phys. Chem. **2**, 2912 (2011).

[35] A. Kelly and Y.M. Rhee, J. Phys. Chem. Lett. **2**, 808 (2011).

[36] J. Strümpfer and K. Schulten, J. Chem. Phys. **131**, 225101 (2009).

[37] X. Chen and R.J. Silbey, J. Phys. Chem. B. **115**, 5499 (2011).

[38] A. Ishizaki and G.R. Fleming, J. Phys. Chem. B. **115**, 6227 (2011).

[39] X. Chen and R.J. Silbey, J. Chem. Phys. **132**, 204503 (2010).

[40] P. Huo and D.F. Coker, J. Chem. Phys **136**, 115102 (2012).

[41] A. Ishizaki and G.R. Fleming, J. Chem. Phys. **130**, 234111 (2009).

[42] M. Thoss, W.H. Miller and G. Stock, J. Chem. Phys. **112**, 10282 (2000).

[43] S. Bonella, D. Montemayor and D.F. Coker, Proc. Natl. Acad. Sci. **102**, 6715 (2005).

[44] E. Martin-Fierro and E. Pollak, J. Chem. Phys. **126**, 164108 (2007).

[45] H. Kim, A. Nassimi and R. Kapral, J. Chem. Phys. **129**, 084102 (2008).

[46] A. Nassimi and R. Kapral, Can. J. Chem. **87**, 880 (2009).

[47] P. Huo, S. Bonella, L. Chen and D.F. Coker, Chem. Phys. **370**, 87 (2010).

[48] H. Wang, M. Thoss and W.H. Miller, J. Chem. Phys. **112**, 47 (2000).

[49] H. Wang, M. Thoss, K.L. Sorge, R. Gelabert, X. Giménez and W.H. Miller, J. Chem. Phys. **114**, 2562 (2001).

[50] G. Tao and W.H. Miller, J. Chem. Phys. **130**, 184108 (2009).

[51] Y. Volobev, M.D. Hack, M.S. Topaler and D.G. Truhlar, J. Chem. Phys. **112**, 9716 (2000).

[52] M.D. Hack and D.G. Truhlar, J. Phys. Chem. A. **104**, 7917 (2000).

[53] S. Bonella, G. Ciccotti and R. Kapral, Chem. Phys. Lett. **484**, 399 (2010).

[54] P. Huo and D.F. Coker, J. Phys. Chem. Lett. **2**, 825 (2011).

[55] H. Lee, Y.C. Cheng and G.R. Fleming, Science **316**, 1462 (2007).

[56] G.S. Engel, T.R. Calhoun, E.L. Read, T.-K. Ahn, T. Mancal, Y.-C. Cheng, R.E. Blankenship and G.R. Fleming, Nature **446**, 782 (2007).

[57] G. Panitchayangkoona, D. Hayes, K.A. Fransted, J.R. Caram, E. Harel, J. Wen, R.E. Blankenship and G.S. Engel, Proc. Natl. Acad. Sci. **107**, 12766 (2010).

[58] E. Collini, C.Y. Wong, K.E. Wilk, P.M.G. Curmi, P. Brumer and G.D. Scholes, Nature **463**, 644 (2010).

[59] A. Ishizaki and G.R. Fleming, Proc. Natl. Acad. Sci. **106**, 17255 (2009).

[60] J. Zhu, S. Kais, P. Rebentrost and A. Aspuru-Guzik, J. Phys. Chem. B. **115**, 1531 (2011).

[61] J. Moix, J. Wu, P. Huo, D.F. Coker and J. Cao, J. Phys. Chem. Lett. **2**, 3045 (2011).

[62] P. Huo and D.F. Coker, Partial linearized density matrix dynamics study of excitation energy transfer and charge separation in a model of photosystem II, in preparation (2012).

[63] T.C Berkelbach, T.E. Markland and D.R. Reichman, J. Chem. Phys. **136**, 084104 (2012).

[64] J. Subotnik, J. Chem. Phys. **132**, 134112 (2010).

[65] W.H. Miller and C.W. McCurdy, J. Chem. Phys. **69**, 5163 (1978).

[66] C.W. McCurdy, H.D. Meyer and W.H. Miller, J. Chem. Phys. **70**, 3177 (1979).

[67] X. Sun and W.H. Miller, J. Chem. Phys. **106**, 6346 (1997).

[68] X. Sun, H. Wang and W.H. Miller, J. Chem. Phys. **109**, 7064 (1998).

[69] D.E. Makarov and N. Makri, Chem. Phys. Lett. **221**, 482 (1994).

[70] R. Egger and C.H. Mak, Phys. Rev. B. **50**, 15210 (1994).

[71] K. Thompson and N. Makri, J. Chem. Phys. **110**, 1343 (1999).

[72] A. Golosov and D.R. Reichman, J. Chem. Phys. **114**, 1065 (2001).

[73] B. Balzer, S. Dilthey, S. Hahn, M. Thoss and G. Stock, J. Chem. Phys. **119**, 4204 (2003).

[74] G. Stock, J. Chem. Phys. **103**, 10015 (1995).

[75] S. Hahn and G. Stock, J. Chem. Phys. **116**, 1085 (2002).

[76] I. Uspenskiy, B. Strodel and G. Stock, Chem. Phys. **329**, 109 (2006).

[77] P. Huo and D.F. Coker, Consistent schemes for non-adiabatic dynamics derived from partial linearized density matrix propagation, in preparation (2012).

Appendix A: Meyer–Miller mapping Hamiltonian formulation [65,66]

One way to avoid the "inverse potential problem" is using the classical analogy of the original Hamiltonian as was suggested in the original work of Meyer and Miller [65,66]. In this work the electronic wave function in the diabatic electronic representation is $|\Psi(R,t)\rangle = \sum_{\lambda} c_{\lambda}(R,t)|\lambda\rangle$, and by inverting the Heisenberg correspondence principle [65,66], they find the electronic coefficients can be rewritten in terms of real variables $\{n_{\lambda}(R,t), \theta_{\lambda}(R,t)\}$: $c_{\lambda} = \sqrt{n_{\lambda}(R,t)}e^{-i\theta_{\lambda}(R,t)}$. This leads to the following Hamiltonian: $H(n,\theta,t) = \sum_{\lambda,\beta} \times \langle\Psi(R,t)|H_{\lambda,\beta}(R,t)|\Psi(R,t)\rangle = \sum_{\lambda,\beta} c^{*}_{\lambda}(R,t)H_{\lambda,\beta}(R,t)c_{\beta}(R,t) = \sum_{\lambda,\beta} \sqrt{n_{\lambda}(R,t)n_{\beta}(R,t)} \quad \cos\big(\theta_{\lambda}(R,t) - \theta_{\beta}(R,t)\big)H_{\lambda,\beta}(R,t)$. Through a canonical transformation from the action-angle variables $(n_{\lambda},\ \theta_{\lambda})$ to the corresponding Cartesian variables

(q_λ, p_λ) by $q_\lambda = \sqrt{2n_\lambda}\cos\theta_\lambda$ and $p_\lambda = -\sqrt{2n_\lambda}\sin\theta_\lambda$, and adding the nuclear kinetic energy term, they arrive at the "classical mapping Hamiltonian" as [67]:

$$H_m^{cl} = \frac{P^2}{2M} + \frac{1}{2}\sum_\beta H_{\beta,\beta}(R)(p_\beta^2 + q_\beta^2) + \frac{1}{2}\sum_{\lambda\neq\beta} H_{\beta,\lambda}(R)(p_\beta p_\lambda + q_\beta q_\lambda). \tag{A1}$$

This is essentially the original mapping Hamiltonian without the "$-\hbar$" term on the diagonal. Following the argument of Meyer and Miller [65,66], there should be "Langer modification" terms to Equation (A1) which subtracts out the term $\frac{1}{2}\sum_\beta H_{\beta,\beta} = \frac{1}{2}tr(H)$ and results in the original mapping Hamiltonian Equation (1).

Appendix B: LAND-map and ILDM propagation: An alternative approach for linearizing the path integral phase

In this appendix we outline the linearized approach to non-adiabatic dynamics in the mapping formulation or LAND-map approach [16] and its iterative implementation known as iterative linearized density matrix (ILDM) propagation [26,47] and highlight the differences in the linearization approaches adopted in these earlier methods compared with the present PLDM approach developed in this paper. The developments of PLDM and LAND-map proceed identically up to Equation (5). Instead of directly apply the linearized approximation to the classical Hamiltonian as is done here with PLDM leading to Equation (6), in the development of the LAND-map equations we first cancel the boundary terms using the following exact relation for the classical mapping Hamiltonian:

$$L_1^{cl} = \sum_\beta p_\beta \dot{q}_\beta - \hat{h}_{map}^{cl}(R) = \frac{1}{2}\frac{\mathrm{d}}{\mathrm{d}\tau}\left(\sum_\beta p_\beta q_\beta\right) \tag{B1}$$

and use a similar result evaluated along the R' path to cancel the boundary terms in the backward path mapping variables. With the PLDM approach we make the assumption that both p_β, q_β and $p'_{\beta'}$, $q'_{\beta'}$ propagate according to the mapping Hamiltonian evaluated along the mean path, $\hat{h}_{map}^{cl}(\bar{R})$, which leads to the approximation: $\sum_\beta p_\beta \dot{q}_\beta - \hat{h}_{map}^{cl}(\bar{R}) = \frac{1}{2}\frac{\mathrm{d}}{\mathrm{d}\tau}\left(\sum_\beta p_\beta q_\beta\right)$. With LAND-map, on the other hand, the forward and backward mapping phase space points propagate according to $\hat{h}_{map}^{cl}(R)$ and $\hat{h}_{map}^{cl}(R')$ respectively. With LAND-map we use the cancellation between the action phase $e^{\frac{i}{\hbar}S_1^{cl}(R,t)} = e^{\frac{i}{\hbar}\int_0^t L_1^{cl}(\tau)\mathrm{d}\tau} = e^{\frac{i}{2\hbar}\int_0^t \frac{\mathrm{d}}{\mathrm{d}\tau}\left(\sum_\beta p_\beta q_\beta\right)\mathrm{d}\tau} = e^{\frac{i}{2\hbar}\sum_\beta(p_{\beta t}q_{\beta t} - p_{\beta 0}q_{\beta 0})}$

and the boundary terms in Equation (4). Thus, with PLDM the action phase and the boundary terms cancel only to zeroth order whereas with LAND-map the total action phase cancels the boundary terms exactly. Now with LAND-map the propagators in Equation (4) can be expressed as (with $\hbar = 1$):

$$T_{[n_t,\, n_0]} = \int \mathrm{d}q_0 \mathrm{d}p_0 \frac{1}{4}(q_{n_t} + ip_{n_t})(q_{n_0} - ip_{n_0})e^{-\frac{1}{2}\sum_\beta (q_{\beta 0}^2 + p_{\beta 0}^2)} \tag{B2}$$

with a similar expression for the backward propagator. To make the linearization approximation in LAND-map, we have to linearize the quantities $p_\beta(R)$, $q_\beta(R)$ and $p_{\beta'}(R')$, $q_{\beta'}(R')$ by expanding their dependence on the environmental DOF about the mean of the forward and backward nuclear paths, $\bar{R}$, in the nuclear path difference, $Z = (R - R')$. Also, we want the overall integrand phase factor to have the form $e^{i\times factor\times Z}$, so that later we can perform the integral dZ over the path difference and obtain δ-functions containing the mean path variables. Based on these considerations, in the development of the LAND-map approach we next introduce the polar representation of the mapping variables, which is closely related to the action angle variables used by Meyer and Miller [65,66] as outlined in Appendix A:

$$\begin{aligned} r_{t,n_t}(\{R_k\}) &= \sqrt{q_{t,n_t}^2(\{R_k\}) + p_{t,n_t}^2(\{R_k\})} \\ \Theta_{t,n_t}(\{R_k\}) &= \tan^{-1}\left(\frac{p_{t,n_t}(\{R_k\})}{q_{t,n_t}(\{R_k\})}\right). \end{aligned} \tag{B3}$$

A more explicit form of Equation (B3) can be obtained using Hamilton's equation of motion for p_{t,n_t} and q_{t,n_t} determined by $\hat{h}_{map}^{cl}(R)$, giving the exact result:

$$\Theta_{t,n_t}(\{R_k\}) = \tan^{-1}\left(\frac{p_{0,n_t}}{q_{0,n_t}}\right) - \int_0^t \mathrm{d}\tau h_{n_t,n_t}(R_\tau) - \int_0^t \mathrm{d}\tau \sum_{\lambda\neq n_t}\left[h_{n_t,\lambda}(R_\tau)\frac{(p_{\tau n_t}p_{\tau\lambda} + q_{\tau n_t}q_{\tau\lambda})}{(p_{\tau n_t}^2 + q_{\tau n_t}^2)}\right]. \tag{B4}$$

With the LAND-map approach we take the full expression for the evolution of the density matrix that contains a phase factor in the difference in phases between the forward and backward paths $[\Theta_{t,n_t}(\{R_k\}) - \Theta'_{t,n'_t}(\{R'_k\})]$ and expand this about the mean path $\bar{R} = (R + R')/2$ to linear order in the difference between the forward and backward paths, Z. The standard assumptions underlying the stationary phase approximation to an oscillatory integral are made including: (1) The pre-exponential amplitude factors are assumed to vary slowly compared to the phase factor so are approximated by their values at the stationary phase points, *i.e.* we assume that $r_{t,n_t}(\{R_k\})$ and $r'_{t,n'_t}(\{R'_k\})$ can be well represented by $r_{t,n_t}(\{\bar{R}_k\})$ and $r'_{t,n'_t}(\{\bar{R}_k\})$, and (2) the time evolution of p_{t,n_t}, q_{t,n_t} and p'_{t,n'_t} and q'_{t,n'_t} are governed by the Hamiltonian $\hat{h}_{map}^{cl}(\bar{R})$, not $\hat{h}_{map}^{cl}(R)$ and $\hat{h}_{map}^{cl}(R')$ respectively. With the present PLDM approach developed in this paper, we make a similar approximation, but with PLDM we do this before we linearize the integrand in the difference between R and R'.

Within the LAND-map development, the above approximations enable us to perform the integrals over Z of the linearized integrand analytically and result in equations of motion for the forward–backward mean paths, $\bar{R}$, that depend on the state labels (n_t, n'_t), governed by classical-like forces that, similarly, are indexed by state labels. The final expression for the density matrix elements is similar to Equation (8), except, now with the LAND-map approach, the forces are state dependent due to our linearization of the particular state dependent angle variables:

$$\begin{aligned} F_k^{n_t,n'_t} = &-\frac{1}{2}\left\{\nabla_{\bar{R}_k}h_{n_t,n_t}(\bar{R}_k) + \nabla_{\bar{R}_k}h_{n'_t,\,n'_t}(\bar{R}_k)\right\} \\ &-\frac{1}{2}\sum_{\lambda\neq n_t}\nabla_{\bar{R}_k}h_{n_t,\lambda}(\bar{R}_k)\left\{\frac{(p_{n_tk}p_{\lambda k} + q_{n_tk}q_{\lambda k})}{(p_{n_tk}^2 + q_{n_tk}^2)}\right\} \\ &-\frac{1}{2}\sum_{\lambda\neq n'_t}\nabla_{\bar{R}_k}h_{n'_t,\,\lambda}(\bar{R}_k)\left\{\frac{(p'_{n'_tk}p'_{\lambda k} + q'_{n'_tk}q'_{\lambda k})}{(p'2_{n'_tk} + q'2_{n'_tk})}\right\}. \end{aligned} \tag{B5}$$

This LAND-map [16] approach has been used to provide an approximate propagator for a short time segment and can be extended by iterating the short time propagator for multiple time slices in the spirit of the development of a path integral approach. This is the so-called iterative linearized density matrix (ILDM) propagation method [26]. Between the short segments, Monte Carlo importance sampling is used to choose a specific pair of state labels that give the most significant contribution to the propagation. These new states are used to initialize the next iteration in the propagation, making the algorithm have the good characteristics of a surface hopping approach, that includes evolution of segments both with forces that represent those present during propagation of populations and different forces that evolve the off-diagonal coherence terms.

One should note that the LAND-map force given above cannot be generated from the original or classical mapping Hamiltonian. This means that with the LAND-map and ILDM propagation approaches the mapping variable and nuclear trajectories are not governed by a single Hamiltonian [16]. This is quite different compared to the present PLDM propagation approach developed in this paper and other semi-classical approaches where the force is generated from the mapping Hamiltonian [44–46,67,68]. It is also different from the Pechukas semi-classical approach of non-adiabatic dynamics [1], where the transition amplitude and trajectory must be determined by self-consistent iteration [29].